

A novel method to analyze the contact resistance effect on OTFTs*

Chen Jinhua(陈金伙)^{1,†}, Hu Jiaying(胡加兴)², and Zhu Yunlong(朱云龙)²

¹School of Physics & Information Engineering, Fuzhou University, Fuzhou 350108, China

²School of Materials Science & Engineering, Xi'an Jiaotong University, Xi'an 710049, China

Abstract: This paper aims to obtain some “universal method and result” to quantitatively analyze the influence of contact resistance (CR) on OTFTs, which has not been reported up to now. This is partly achieved by means of the simulated method and the introduction of R_c/R_{ch0} (the value of CR/on state channel resistance). To do this, the OTFT formula from the Brown model is extended, and the parameter (errors carrier mobility μ , saturation voltage V_{Dsat} , etc.) caused by R_c are analyzed in detail. Then, the R_c/R_{ch0} test method is emphatically demonstrated, and some meaningful conclusions are drawn. Based on the conclusion, it is the first time that a “universal method” of estimating the errors caused by R_c has been put forward. Experimental results further prove that the method is correct.

Key words: OTFT; numerical study; I_{on}/I_{off} ; ohmic contact; error analysis

DOI: 10.1088/1674-4926/33/12/124005

PACC: 7280L; 7340C; 7310R

1. Introduction

Great achievements have been made in the past twenty years in the organic thin film transistor (OTFT) field^[1], and they are now widely used in AMOLEDs, intelligent cards, IF logic circuits^[2-4], etc. With the performance of OTFTs being greatly enhanced^[5,6], the contact resistance (CR) that widely exists in OTFTs, began to play an increasingly unfavorable role, resulting in high work voltage, low carrier mobility, etc.^[7,8]. Nevertheless, the CR effect is seldom discussed in detail, which not only results from the complexity of the CR generation mechanism, such as the mismatched work function among materials and interface located state concentration variation with V_G/V_D ^[9,10], but also results from the serious relevance of the CR effect with many parameters, e.g., the channel length (L), the channel width (Z), the carrier mobility μ , and the dielectric constant of materials. These factors made the conclusion obtained in many papers to be less meaningful, namely, one conclusion could be suited for this OTFT, but it may not for another. Therefore, it is quite important to develop one “universal method” that can be used in all papers to analyze the CR effect, which has not been achieved up to now.

To solve this problem, one key parameter, R_c/R_{ch0} (R_c /on state channel resistance of OTFT) was adopted and analyzed in detail. It was found to play important role in analyzing the CR effect. By means of R_c/R_{ch0} , not only was its relationship with OTFT performance parameters (μ , I_{on}/I_{off} , V_{Dsat} , etc) demonstrated, but also its test methods. It was significantly noted that the results were suitable for all OTFTs. To fulfill this, the formula of the Brown model for OTFTs^[4-11] was extended, which was critical in this study.

2. Theoretical analysis

In his paper, Brown got the formula of OTFT as follows^[11].

When $V_G < V_D$,

$$\begin{aligned} I_{DS} \int_0^L dx &= I_{DS} L \\ &= Z \int_0^{V_D} \mu \{e N_A d_s - C_i [V_G - V' - V(x)]\} dV. \end{aligned} \quad (1)$$

Finally, the linear formula was:

$$I_{DS} = \frac{Z}{L} \mu C_i \left[(V_0 - V_G) V_D + \frac{1}{2} V_D^2 \right]. \quad (2)$$

When $V_G - V_D < V_p$, I_{DS} is saturated. Brown obtained the equation:

$$\begin{aligned} I_{DS} &= \frac{Z}{L} \mu C_i \left[(V_0 - V_D) V_D + \frac{1}{2} V_D^2 \right] \\ &\quad - \frac{Z \mu e^2 N_A^2 d_s^3}{L \epsilon_s} \frac{d_s^3}{6} \left(1 + 3 \frac{C_s}{C_i} \right). \end{aligned} \quad (3)$$

When $0 < V_G - V_D < V_p$, Brown did not show the related formula, but rewrote Eq. (1) as:

$$\begin{aligned} I_{DS} &= \frac{Z}{L} \int_0^{V_G} \mu \{e N_A d_s - C_i [V_G - V' - V(x)]\} dV \\ &\quad + \frac{Z}{L} \int_{V_G}^{V_D} \mu e N_A [d_s - W(V)] dV. \end{aligned} \quad (4)$$

Here, it was further deduced by the depletion thickness literature^[12]:

* Project supported by the Fujian Natural Science Foundation, China (No. 2009J05146).

† Corresponding author. Email: pt_sky@163.com

Received 23 July 2012, revised manuscript received 29 September 2012

$$W(V) = \frac{\epsilon_s}{C_i} \left[\sqrt{1 + \frac{2C_i^2 |V_G - V(x)|}{qN_A \epsilon_s}} - 1 \right]. \quad (5)$$

Obviously, $V(x)$ was related to variable $W(V)$, thus it was changed as:

$$\begin{aligned} V(x) &= V_D \rightarrow W(V_D) = d'_s \\ &= \frac{\epsilon_s}{C_i} \left[\sqrt{1 + \frac{2C_i^2 |V_G - V_D|}{qN_A \epsilon_s}} - 1 \right], \\ V(x) &= V_G \rightarrow W(V_G) = 0, \\ V_{\text{Sat}} &\rightarrow W = d_s, \\ dV &\rightarrow -\frac{1}{C_i} N_A q \left[1 + \frac{C_i}{\epsilon_s} d_s(V) \right] dW. \end{aligned} \quad (6)$$

Thus Equation (4) was changed as:

$$\begin{aligned} I_{\text{DS}} &= \frac{Z}{L} \mu C_i \left[(V_0 - V_G) V_G + \frac{1}{2} V_G^2 \right] \\ &\quad - \frac{Z \mu q^2 N_A^2}{L \epsilon_s} \int_0^{d'_s} (d_s - W) \left(W + \frac{\epsilon_s}{C_i} \right) dW. \end{aligned} \quad (7)$$

By integrating the above formula, it finally obtained:

$$\begin{aligned} I_{\text{DS}} &= \frac{Z}{L} \mu C_i \left[(V_0 - V_G) V_G + \frac{1}{2} V_G^2 \right] \\ &\quad - \frac{Z \mu q^2 N_A^2}{L \epsilon_s} \left[\frac{\epsilon_s}{C_i} d_s d'_s + \frac{1}{2} \left(d_s - \frac{\epsilon_s}{C_i} \right) d_s^2 - \frac{1}{3} d_s^3 \right]. \end{aligned} \quad (8)$$

3. Experiments

To testify the validity of the method, two top-contact OTFTs were fabricated under the same condition in this work. For simplicity, the heavily doped silicon wafer, which was covered by one silicon dioxide layer of 300 nm, was directly used as the substrate/gate electrodes and gate dielectric. In sequence, the wafer was ultrasonically cleaned in acetone solution, ethanol solution and deionized water for 10 min, respectively. Then it was treated by UV for 10 min, and further it was moved to one chamber to prepare a 100 nm thickness Pentacene layer to act as the semiconductor layer by the thermal evaporation method under a pressure of 5×10^{-3} Pa and an evaporated rate of 0.3 Å/s. Subsequently, the devices were moved to another chamber to deposit 50 nm gold (Au) film as the source/drain electrode under 4×10^{-3} Pa through a shadow mask. The channel width (Z) of 3.6 cm and the channel lengths (L) of 20 μm were obtained. Furthermore, the material thickness was measured by a step profiler, and the relevant electrical characteristics of the OTFTs were measured by using a Keithley 4200 source meter in air at room temperature, respectively.

In addition, two resistances of $R_{\text{out}1} = 0 \Omega$, $R_{\text{out}2} = 2 \times 10^4 \Omega$ were connected to these two OTFTs (OTFT1 and

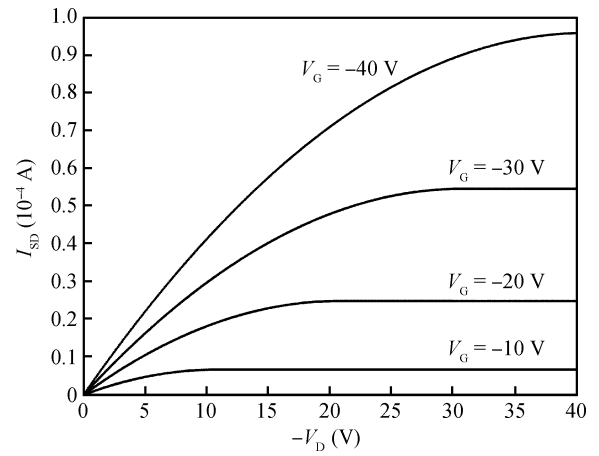


Fig. 1. I - V characteristic curves of the OTFT with $R_c = 0 \Omega$.

OTFT2) to act as the contact resistance, respectively. It was helpful to analyze the influence of R_c on OTFT, which will be demonstrated later.

4. Results and discussion

4.1. Theoretical results

By the formula deduced in Section 2, a numerical study on OTFTs was carried out, in which the parameters were adopted as: channel width $Z = 3.6$ mm, channel length $L = 20 \mu\text{m}$, thickness of active (d_s)/insulator layers (d_i) = 100 nm/300 nm, relative inductivity of semiconductor (ϵ_s)/of insulator material (ϵ_i) was 2.2/3.5, impurity concentration $N_A = 5.0 \times 10^{15} \text{ m}^{-3}$, carrier mobility $\mu = 3.1 \times 10^{-3} \text{ cm}^2/(\text{V}\cdot\text{s})$, and R_c was zero.

Figure 1 plotted the I - V curves of the OTFT under different gate voltages V_G , in which the linear curve and saturated I - V curve were perfectly connected, indicating the important role of transition formula deduced in Section 2. Furthermore it suggested that the deduction in Section 2 was correct.

4.2. Numerical results and analysis

As expected, $R_c/R_{\text{ch}0}$ was found to be one key parameter to exclude the influence of the many factors mentioned above, which was demonstrated as follows:

Firstly, Figure 2 plotted the relationship of $\Delta\mu/\mu$ (μ in linear region) with $R_c/R_{\text{ch}0}$. Significantly, it was noted that the curve in Fig. 2 was independent of nearly all the parameters that appeared in Brown formula in Section 2, i.e., it was not only irrelevant with the working condition (V_G and V_D) and the structural parameters (Z , L , d_s , d_i , etc.) of the OTFT, but also irrelevant with the material parameters (relative inductivity ϵ_s , ϵ_i) and the film quality (the carrier mobility μ), etc.

In other words, by virtue of the parameter $R_{\text{ch}0}$, and the method to analyze the relationship between $\Delta\mu/\mu$ with $R_c/R_{\text{ch}0}$, the “universally applicable result” of CR influence on μ could be obtained in Fig. 2. Obviously, the result is helpful to calculate the real μ in the linear region for the OTFT once the real $R_c/R_{\text{ch}0}$ is obtained.

The correctness of Fig. 2 was further proved by experiment, which will be demonstrated later in detail. In our experiment, no matter how much “outside” resistance was connected

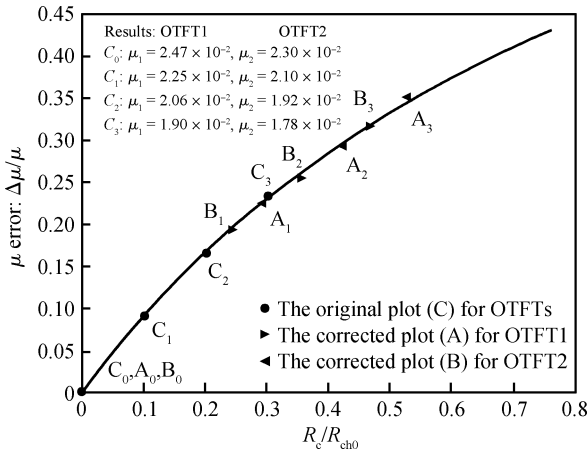


Fig. 2. Relationship of $\Delta\mu/\mu$ with R_c/R_{ch0} .

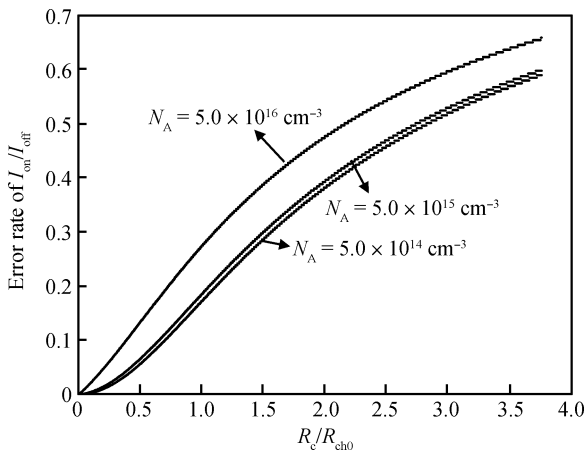


Fig. 3. Error rate of I_{on}/I_{off} varied with R_c/R_{ch0} .

to the source electrode (C_i point, $i = 1, 2, 3$), and whether the “inner” resistance existing in OTFT was taken into account, the plots (A_i, B_i, C_i points, $i = 1, 2, 3$) all distributed along the solid line in Fig. 2. The accordance of A_i, B_i, C_i with the solid line further indicated that the result in Fig. 2 was universally applicable.

Expected for μ error, the error of I_{on}/I_{off} ratio caused by R_c was qualitatively analyzed. Taking into account that the channel resistance in the “off” state was far bigger than that in the “on” state, the change of I_{on}/I_{off} mainly originated from I_{on} , thus the relationship curve of I_{on}/I_{off} with R_c/R_{ch0} was plotted in Fig. 3 (in which $V_D = V_G$ was applied in the on state).

Comparing with Fig. 2, it could be seen that the error of the I_{on}/I_{off} ratio was much smaller than that of μ error under the same R_c . Furthermore, the change of I_{on}/I_{off} was found to sensitively rely on N_A once $N_A > 5 \times 10^{14} \text{ cm}^{-3}$ in this circumstance. Otherwise, it nearly kept unchangeable.

Furthermore, the saturation voltage (V_{Dsat}) error by R_c was analyzed too. The ratio of $\Delta V_{Dsat}/V_{Dsat}$ was found to be linearly related with R_c/R_{ch0} (the solid line). Usually, the slope coefficient (parameter K) in Fig. 4 was taken as a variable, while here something meaningful was obtained.

To study the important parameter K , simulation method was further used, and it was interesting to find that: though K varied with many parameters, there was one max limit value

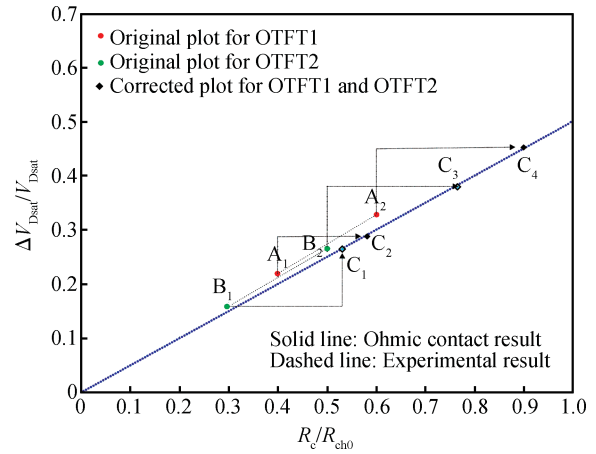


Fig. 4. Relationship of $\Delta V_{Dsat}/V_{Dsat}$ with R_c/R_{ch0} .

of K ($K_{max} = 0.5$), as presented in Fig. 4. Simulated results showed that no matter what parameter in the Brown formula changed, K was decreased to some extent. As for the change trend, the numerical result further indicated that: K was slightly/mainly decreased with the increase of ϵ_i and the decrease of d_i /with the increase of N_A, d_s and the decrease of ϵ_s , expected that, K was totally irrelevant with channel length L , channel width Z , and carrier mobility μ .

Based on the above results, the minimum value of K (K_{min}) was studied too. Obviously, K_{min} can be obtained when the max d_s, ϵ_i and the min ϵ_s, d_i are adopted. Here, the min value of $\epsilon_s = 2, d_i = 50 \text{ nm}$ and the max value of $d_s = 200 \text{ nm}, \epsilon_i = 10$ in the common parameter range for contemporary OTFTs was used. On this premise, K_{min} varied with N_A , as plotted in Fig. 5(a).

In Fig. 5(a), K_{min} evidently approached K_{max} ($1/2$) under $N_A < 2 \times 10^{15} \text{ cm}^{-3}$. This result indicated that: the error of K (by adoption of $K = 1/2$) is nearly equal to zero, i.e., the conclusion of $K = 1/2$ was suitable for nearly all contemporary OTFTs with $N_A < 2 \times 10^{15} \text{ cm}^{-3}$.

When $N_A > 2 \times 10^{15} \text{ cm}^{-3}$, K_{min} was decreased to some extent. Under this circumstance, Figure 5(b) showed that K_{min} depended not only on N_A but also on d_s . Moreover, with a higher N_A , more serious error was produced by $K = 1/2$, and the “max” error of K can be further estimated in Fig. 5(b). For example, if $N_A = 4 \times 10^{15} \text{ cm}^{-3}$, the conclusion that the max error of K (by $K = 1/2$) was less than 5% can be drawn in Fig. 5(b).

Taking into account of the fact that “organic” material was very difficult to dope, $N_A = 4 \times 10^{15} \text{ cm}^{-3}$ was a quite big value for an OTFT, namely, $K = 1/2$ can be considered as a “universal result” for nearly all contemporary OTFTs, in which N_A was usually less than $4 \times 10^{15} \text{ cm}^{-3}$.

The conclusion above was of great significance, according to which one method to estimate the “real” R_c and R_{ch0} was first put forward.

For OTFT, the OTFT resistance commonly consisted of the channel resistance R_{ch0} and the contact resistance R_c . If the OTFT was taken as the “ohmic contact”, the parameter R'_{ch0} and the voltage V'_{Dsat} can be measured easily (noted that: here R'_{ch0} was not the real R_{ch0} , but the sum of the “real” R_{ch0} and the real R_c ; V'_{Dsat} included the real V_{Dsat} and the voltage on the

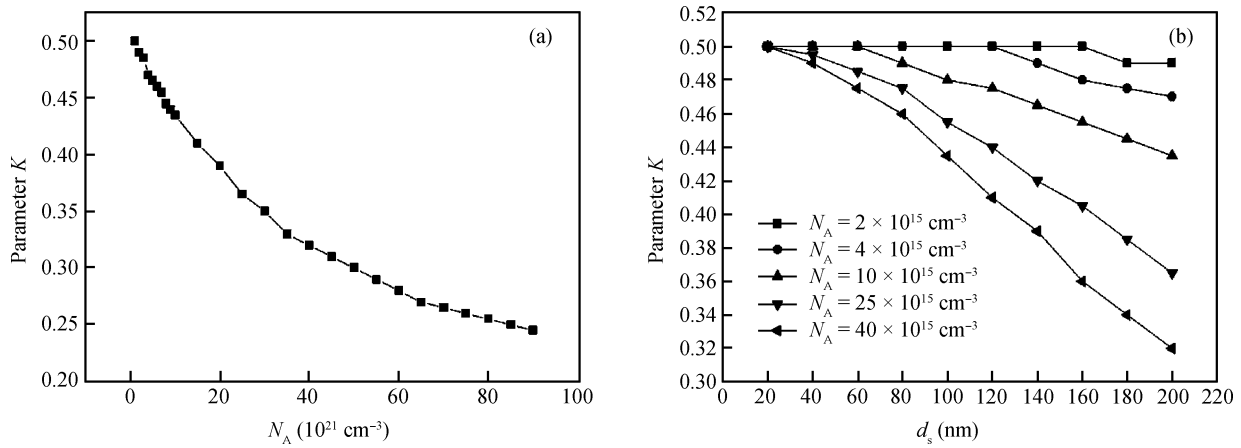


Fig. 5. (a) K_{\min} varied with N_A . (b) K_{\min} varied with d_s when $N_A \geq 2 \times 10^{15} \text{ cm}^{-3}$.

real R_c). Then one adjustable resistance R_{out} was connected to OTFT source electrode to act as the contact resistance R'_c , thus the $\Delta V'_{\text{Dsat}}$ and the plot of $\Delta V'_{\text{Dsat}}/V'_{\text{Dsat}}$ variation with R'_c/R'_{ch0} can be measured easily. Evidently, if the OTFT was an “ohmic contact”, the plot should be in accordance with the solid line in Fig. 4, otherwise, the slope would increase.

4.3. Experimental results and analysis

To test and verify the above conclusion, two OTFTs based on pentacene were made in Section 3. In addition, two resistances $R_{\text{out1}} = 0 \Omega$, $R_{\text{out2}} = 2 \times 10^4 \Omega$ were connected to these two OTFTs (OTFT1 and OTFT2) to act as the R'_c , respectively. The experimental results ($\Delta\mu/\mu$ and $\Delta V'_{\text{Dsat}}/V'_{\text{Dsat}}$ that varied with R'_c/R'_{ch0}) were plotted in Fig. 2, in which points A and B were ascribed to OTFT1 and OTFT2, respectively.

In Fig. 4, the slopes of curves A and B (dashed line) were both greater than 1/2, indicating the real $R_c \neq 0$ existing in these two OTFTs. By using the method mentioned above, the real R_c of $R_{c1} \approx 8.5 \times 10^4 \Omega$ for OTFT1 and $R_{c2} \approx 1.15 \times 10^5 \Omega$ for OTFT2 were then obtained. According to R_{c1} and R_{c2} , the nearly equivalent R_{ch0} for OTFT1 and OTFT2 can be obtained. Moreover, by R_{c1} and R_{c2} , the positions of A_1 and A_2 , B_1 and B_2 were corrected at C_1, C_2, C_3, C_4 , respectively. Evidently, the corrected results (nearly equal R_{ch0} and points C_1, C_2, C_3, C_4 located along the solid line in Fig. 4) were more in line with the fact that OTFT1 and OTFT2 were made under the same conditions. This further indicated that the method mentioned above was reasonable.

By R_{c1} and R_{c2} , the results in Fig. 2 were further corrected. As shown in Fig. 2, $\mu_1 = 2.47 \text{ cm}^2/(\text{V}\cdot\text{s})$ for OTFT1 and $\mu_2 = 2.31 \text{ cm}^2/(\text{V}\cdot\text{s})$ for OTFT2 were calculated under $R_{\text{out}} = 0$. Here, the influence of R_c was further taken into account. By substituting the assumed R_c ($R_c = 0$) with the real R_c ($R_{c1} \approx 8 \times 10^4 \Omega$ and $R_{c2} \approx 1.2 \times 10^5 \Omega$ were obtained above), the real $\mu_1 = 2.78 \text{ cm}^2/(\text{V}\cdot\text{s})$ and $\mu_2 = 2.72 \text{ cm}^2/(\text{V}\cdot\text{s})$ were obtained for OTFT1 and OTFT2, respectively. Evidently, the corrected results ($\Delta\mu$ ($\Delta\mu = 0.06 \text{ cm}^2/(\text{V}\cdot\text{s})$) were much smaller than the original result ($\Delta\mu = 0.16 \text{ cm}^2/(\text{V}\cdot\text{s})$), it was closer because OTFT1 and OTFT2 were fabricated under nearly the same experimental conditions. Together with the results from Fig. 4 (nearly equal R_{ch0} and the points C_1, C_2, C_3, C_4 dis-

tributed along the solid line), all these results suggested that the corrected method was scientific.

Furthermore, it was noticed that either the original point ($C_i, i = 1, 2, 3$) or the corrected points ($A_i, B_i, i = 1, 2, 3$) in Fig. 2 were all distributed along the solid line, it further indicated that the conclusion in Fig. 2 was a universal result, it was independent of all parameters in the Brown formula, thus it was “universally applicable”.

5. Conclusion

Some “universal results” for OTFTs and one “universal test method” for current OTFTs ($N_A < 2 \times 10^{15} \text{ cm}^{-3}$) to quantitatively analyze the CR influence on OTFTs were simultaneously obtained in this paper. Firstly, the universal results of the CR influence on OTFTs were plotted in Figs. 2–4. Furthermore, the curve of K that varied with N_A, d_s was analyzed in detail and the conclusion that $K = 1/2$ was suitable for nearly all contemporary OTFTs was drawn. By the conclusion, one “universally applicable method” to analyze the influence on OTFTs was presented for the first time. Both the analyzed results and the correction method were further proved to be correct by the experiment results, indicating that they were of great significance to many papers, in which the CR effect was perhaps noticed but not corrected due to the absence of a relating “universal” result and correction method for OTFTs.

References

- [1] Koezuka H, Tsumura A, Koezuka T H, et al. Field-effect transistor with polythiophene thin film. *Synthetic Metals*, 1987, 18: 699
- [2] Ryu G S, Choe K B, Song C K. Array of organic thin film transistors integrated with organic light emitting diodes on a plastic substrate. *Thin Solid Films*, 2006, 514: 302
- [3] Fadlallah M, Billiot G, Eccleston W. DC/AC unified OTFT compact modeling and circuit design for RFID applications. *Solid-State Electron*, 2007, 51: 1047
- [4] Wang W, Ma D, Gao Q. Organic thin-film transistor memory with Ag floating-gate. *Microelectron Eng*, 2012, 91: 9
- [5] Park E Y, Park J S, Kim T D, et al. High-performance n-type organic field-effect transistors fabricated by ink-jet printing using a C60 derivative. *Org Electron*, 2009, 10: 1028

- [6] Li Y, Singh S P, Sonar P. A high mobility P-type DPP-Thieno[3,2-b] thiophene copolymer for organic thin-film transistors. *Adv Mater*, 2010, 22: 4862
- [7] Yun D J, Lee D K, Jeon H K, et al. Contact resistance between pentacene and indium-tin oxide (ITO) electrode with surface treatment. *Org Electron*, 2007, 8: 690
- [8] Li J, Zhang X W, Zhang L, et al. Improving organic transistor performance through contact-area-limited doping. *Solid State Commun*, 2009, 149: 1826
- [9] Gao Y. Surface analytical studies of interfaces in organic semiconductor devices. *Mater Sci Eng R*, 2010, 68: 39
- [10] Tanese M C, Fine D, Dodabalapur A, et al. Organic thin-film transistor sensors: Interface dependent and gate bias enhanced responses. *Microelectronics*, 2006, 37: 837
- [11] Brown A R, Jarrettb C P, de Leeuw D M, et al. Field-effect transistors made from solution-processed organic semiconductors. *Synthetic Metals*, 1997, 88: 37
- [12] Horowitz G, Hajlaoui R, Bouchriha H, et al. The concept of threshold voltage in organic field-effect transistors. *Adv Mater*, 1998, 10: 923
- [13] Klauk H, Halik M, Zschieschang U, et al. Pentacene organic transistors and ring oscillators on glass and on flexible polymeric substrates. *Appl Phys Lett*, 2003, 82: 4175